

## 3D reconstruction and visualization from 2D X-ray CT images in the study of ceramic membrane microstructure

Thomasová Barbora<sup>a,b</sup>, Thomas Jan<sup>b</sup>, Souček Kamil<sup>b,c</sup>, Michálek Ondřej<sup>b</sup> and Gembalová Lucie<sup>b</sup>

<sup>a</sup>Nanotechnology Centre, VŠB-Technical University of Ostrava, 17. listopadu 2172/15, Ostrava – Poruba, 708 00, Czech Republic

<sup>b</sup>Institute of Clean Technologies of Extraction and Utilization of Energy Resources, Faculty of Mining and Geology VŠB-Technical University of Ostrava, 17. listopadu 2172/15, Ostrava – Poruba, 708 00 Czech Republic

<sup>c</sup>Institute of Geonics of the CAS, Studentská 1768, Ostrava – Poruba, 708 00 Czech Republic

In the presented study, X-ray computed tomography (CT) technique was used to visualize the three-dimensional (3D) microstructure of ceramic membrane support made of alternative material - fly ash, kaolin and shale. Standard computed tomography output formats provide usually two-dimensional (2D) information about the object being studied in the form of image data set. However, to understand the material internal structure and its mechanical, physicochemical and hydraulic properties 3D visualization is needed. Our work shows that 3D image data reconstruction can be done with freely available DREAM.3D and ParaView software instead of costly commercial ones allowing wider community data sharing and greater freedom in processing. The resulting 3D model was suitable for quantitative pore space analysis and fluid dynamics modelling and provided important morphological information such as pore and mass shape, cracks, spatial distribution and the connectivity of the solid matrix.

**Keywords:** X-ray CT, 3D model, ceramic, DREAM.3D, ParaView.

### Introduction

Ceramic membranes systems used for industrial wastewater treatment, recovery and reuse represent one of the most important technologies that have gained popularity over past two decades. Ceramic membranes for industrial effluent filtration usually consist of three filtration layers, porous support, interlayer and a top layer with different densities and decreasing thickness. All layers can be made of the same or different material. Porosity values of supports and filtration layers depend on the sintering temperature and material used [1-3] and could be up enhanced by pore forming agents up to 60% [4]. Generally, membrane supports have a total porosity ratio of about 40% [2]. Ceramic membranes for the purpose of wastewater treatment belong to the oxide ceramic membranes that are mainly made of Al, Si, Ti or Zr oxides, and silicon carbide [5]. Membranes made of these materials are characterized by high durability, chemical, mechanical and thermal stability, bacteria resistance, and ability of back flushing and ease of cleaning and sterilization [6]. However, their preparation and production is too expensive and therefore a significant effort has been devoted to finding

alternative low cost materials, usually based on natural or waste products [7-10]. Reduction of ceramic membranes fabrication cost is one of the basic parameters enabling wider application in various industrial wastewater treatment plants.

Considering the ceramic membranes costs and with respect to the sustainability of natural resources, tubular geopolymer support made by fly ash from energy coal combustion, kaolin and shale was prepared in this work.

When creating new filtering materials, not only ceramic, the knowledge of the structure of the material plays a significant role. It is well known that the microstructure of the resultant porous material such as porosity, pore size distribution, tortuosity and subsequently the mass transport properties (liquid permeability or fluid distribution) are key parameters for good filtration function [11-13].

Conventionally, microstructural visualization is predominantly based on 2D imaging techniques such as SEM (scanning electron microscopy) and TEM (transmission electron microscopy) however these techniques do not enable access to the actual spatial distribution of pores, their shape, connectivity and inner structure of material.

The X-ray computed tomography (CT) seems to be the most convenient technique that provides all of above-mentioned information. CT is a non-destructive technique that offers three-dimensional characterization

\*Corresponding author:  
Tel : +420 597 325 464  
Fax: +420 596 918 589  
E-mail: lucie.gembalova@vsb.cz

and visualisation of the internal structure of the material by 2D image data reconstruction to form a virtual 3D model. X-ray CT relies on measurement of the attenuation of X-ray passing through a specimen, thereby generating high-resolution radiographs. The magnitude of linear attenuation is dependent on physical density and chemical composition of the material as well as on the X-ray energy [14]. Output CT data is volume discrete data characterizing the structure of the material in the sample. Because the acquired image data does not distinguish individual objects in the scanned sample, it is necessary to proceed with the mathematical analysis of the image data. A number of authors dealt with methods of mathematical analysis of the image data and the creation of a 3D model [14-17]. However, there are not many papers dealing with 3D visualization of the membrane structure. Several works have been devoted to X-ray CT microstructure characterization of inorganic materials such as ceramic fibres, minerals or rocks [18-20].

Nowadays the 3D model reconstruction from 2D image data is usually done with costly specialized commercial software that is closely connected with the specific type of tomograph. This fact limits the possibilities for individual use, freedom in data processing and data sharing in a wider community of users.

One of main aim of this work was an introduction of the methodology for 3D model creation based on utilization of ParaView and DREAM.3D open source software. The whole process of 2D image data processing into 3D model is outlined in the work including application of several mathematical algorithms such as noise reduction, thresholding and region growing method up to final 3D model creation by vectorization, smoothing and decimation. By creating 3D object it was possible to describe the internal structure of ceramic material, its porosity or the defects and failures creating during support preparation. The 3D geometric model also served to assess homogenization of individual components by tracking the size and distribution of particles with a specific property. Fluid dynamics simulation within porous material has been also outlined as other possibility of using 3D geometric model.

## Experimental

### Input material characterization

Three powder materials were used for ceramic support preparation, fly ash from the combustion of energy coal, kaolin as a plasticizer and refractory claystone with its excellent thermal stability and high content of  $\text{Al}_2\text{O}_3$  and plastic binding ability in ceramics. The temperature of combustion process of fly ash was in range of 800 °C. Chemical composition of input materials were characterized by energy-dispersive X-ray fluorescence spectrometry (Spectro XEPOS). For particle size analysis the Partica LA-950 Laser Diffraction

Particle Size Distribution Analyzer HORIBA LA-950 was used.

### Support preparation

Raw input powder materials were mixed together in ratio 2:2:1. Paste suitable for extrusion was made by addition of 5M NaOH. One-channel tubes 150 mm long and 15 mm wide were prepared by manual extruder. Tubes were dried at room temperature for 48 h and then sintered at 1,000 °C for 2 h. In this way, supports suitable for microfiltration were prepared.

### Support characterization methods

Prepared support was characterized by various techniques including scanning electron microscopy (SEM), X-ray diffractometry (XRD) and Mercury porosimetry. SEM images were taken with Scanning Electron Microscope FEI Quanta FEG equipped with electron backscatter diffraction detector (EBSD). For phase identification Bruker Advance D8 was used. Pore size distribution and porosity evaluation was performed using mercury porosimeter Autopore IV 9500.

### X-ray CT measurement

Computed tomography was performed using X-ray micro-CT scanner XTH 225 ST made by NIKON Metrology NV. Microfocus X-ray source is equipped with a 225 kV/225 W reflection target with 3  $\mu\text{m}$  focal spot size up to 7 W of power and with a 180 kV/20 W transmission target with 1  $\mu\text{m}$  focal spot size up to 3 W of power.

Transmission target at 150 kV/3.5 W was used for CT scanning of the ceramic material. Instrument is configured with flat detector Perkin Elmer 1,620 with  $2,000 \times 2,000$  active pixels (pixel size 200  $\mu\text{m}$ , 4 mil. pixels). The ceramic fragment sample was cube of approximate edge length of 5 mm.

For reconstruction of the CT volume of the investigated sample, we acquired 3 141 2D radiographic projections (images) at a known rotational angle during one full sample turn (360°). The exposition time of the one radiographic projection was 4,000 ms consisting of two radiographic frames (2,000 ms). The scanning and reconstruction process of one ceramic porous sample takes approximately five hours and resulting resolution of the individual cubic voxels in CT volume is represented by value of approx. 2.7  $\mu\text{m}$ . (the voxel resolution is directly proportional to the geometrical magnification of the sample on the flat panel X-ray detector). For the primary CT data visualization and preparation of the stack of 2D tomographic slices for following analysis, we used software VG Studio Max v. 2.2. (VGS).

### Reconstruction of 3D model using ParaView and DREAM.3D software

Two software namely ParaView and DREAM.3D, were used for 3D model reconstruction from 2D CT

data (slices). Both are an open-source multi-platform data analysis and visualization applications.

ParaView allows you to quickly create visualizations for user data analysis using qualitative and quantitative techniques. The data exploration can be done interactively in 3D or programmatically using ParaView's batch processing capabilities. ParaView supports distributed computation models to process large data sets and also develops an extensible architecture based on open standards [21].

DREAM.3D consists of data analysis tools (*filters*) that allow for the construction of customized workflows (*Pipelines*) to analyse data. DREAM.3D provides a flexible and extensible data structure that eases data transport between collaborators by storing data in a non-proprietary format. The reconstructions can utilize an array of alignment, cleaning, segmentation algorithms and colouring algorithms. Many algorithms are available to extract various statistics about received data [22].

Mathematical filters (algorithms) of DREAM.3D software were used to process 2D data from X-ray CT. In order to create a three-dimensional model obtained by converting a discrete description of the data obtained by mathematical analysis of 2D image data by DREAM.3D application, both software DREAM.3D and Paraview were used.

## Results and Discussion

### X-ray fluorescence spectrometry

The elemental composition for materials used is given in Table 1. It is evident that the major components in fly ash, kaolin and shale were  $\text{SiO}_2$  and  $\text{Al}_2\text{O}_3$ .

High content of Al and Si ions in raw samples made the mixture suitable for geopolymerization process described by Davidovits [23]. During this process reorganization (destruction) of solid aluminosilicates oxides due to attack of alkali ions occurs, consequently complicated process including precipitation, gel formation, polymerization, hardening and new material formation takes place.

### Particle size distribution

The Fig. 1 shows the particle size distribution of raw input materials. It is evident that except of kaolin whose particle size distribution is within a very narrow range, the particle size distribution of fly ash and shale is in the range of units to hundreds of  $\mu\text{m}$ .

Economic efficiency was the main goal of preparing ceramic support based on waste and natural materials

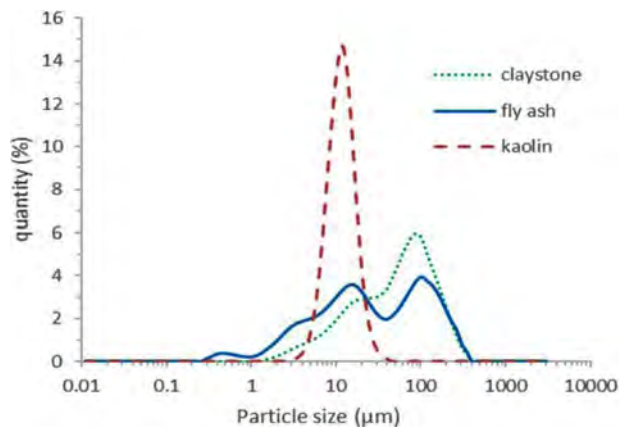


Fig. 1. Particle size distribution of fly ash, kaolin and shale.

and therefore no reduction in particle size (milling) of input materials was intended.

### Scanning electron microscopy

The scanning electron microscope (SEM) images of inner profile of extruded tube before and after sintering are depicted in Fig. 2 and 3. In Fig. 2, are visible ball shaped grains ideal for the preparation of ceramic membrane. After sintering at  $1,000\text{ }^\circ\text{C}$  the individual grains melted and become fused to one another forming porous structure (Fig. 3).

### Phase identification

Phase identification was determined using X-ray diffraction. XRD data for the sintered and unsintered sample are shown in Fig. 4. Semiquantitative composition of input materials was determined by the standard ZnO (Zincite) addition. In unsintered sample the major phases identified was amorphous (49%). The major crystalline phases were in the following order mullite ( $3\text{Al}_2\text{O}_3 \cdot 2\text{SiO}_2$ ), quartz ( $\text{SiO}_2$ ), kaolinite ( $\text{Al}_2\text{Si}_2\text{O}_5(\text{OH})_4$ ), magnetite ( $\text{Fe}_3\text{O}_4$ ) and hematite ( $\text{Fe}_2\text{O}_3$ ). After sintering the sample became more amorphous (55%), kaolinite transformed to mullite (silicate with isolated  $\text{SiO}_4$  tetrahedrons) whose content increased, and other silicate phases – tectosilicates (tetrahedral bounds to a spatial network) nepheline and labradorite were identified. In addition, content of cristobalite (high temperature form of  $\text{SiO}_2$ ) increased. These changes led to creation of a solid porous structure.

### Mercury porosimetry

Mercury (Hg) porosimetry is the basic characterization

Table 1. Chemical composition of materials used for support preparation.

	$\text{Na}_2\text{O}$	$\text{MgO}$	$\text{Al}_2\text{O}_3$	$\text{SiO}_2$	$\text{P}_2\text{O}_5$	$\text{SO}_3$	$\text{K}_2\text{O}$	$\text{CaO}$	$\text{TiO}_2$	$\text{Fe}_2\text{O}_3$	LOI <sup>a</sup>
Fly ash	0.50	1.87	26.1	54.2	0.50	0.25	3.36	2.63	1.13	6.82	2.03
Kaolin [weight. %]	< 0.03	0.15	30.4	55.5	0.06	< 0.01	1.48	< 0.01	1.03	0.53	10.2
Shale	0.03	0.12	41.9	53.4	0.08	0.02	0.67	0.07	1.93	1.11	0.13

<sup>a</sup> Loss of ignition

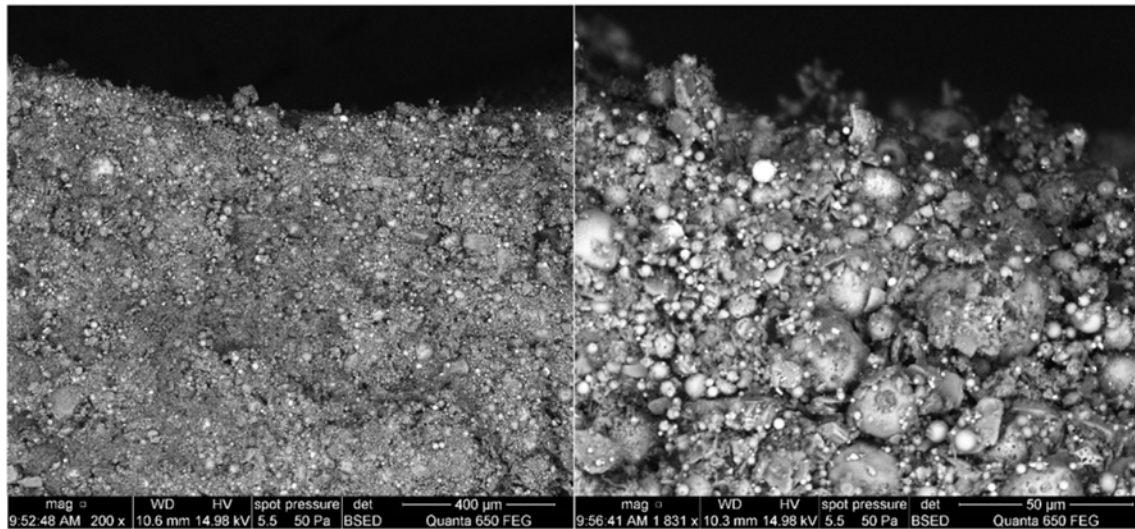


Fig. 2. Inner profile of the extruded tube before sintering.

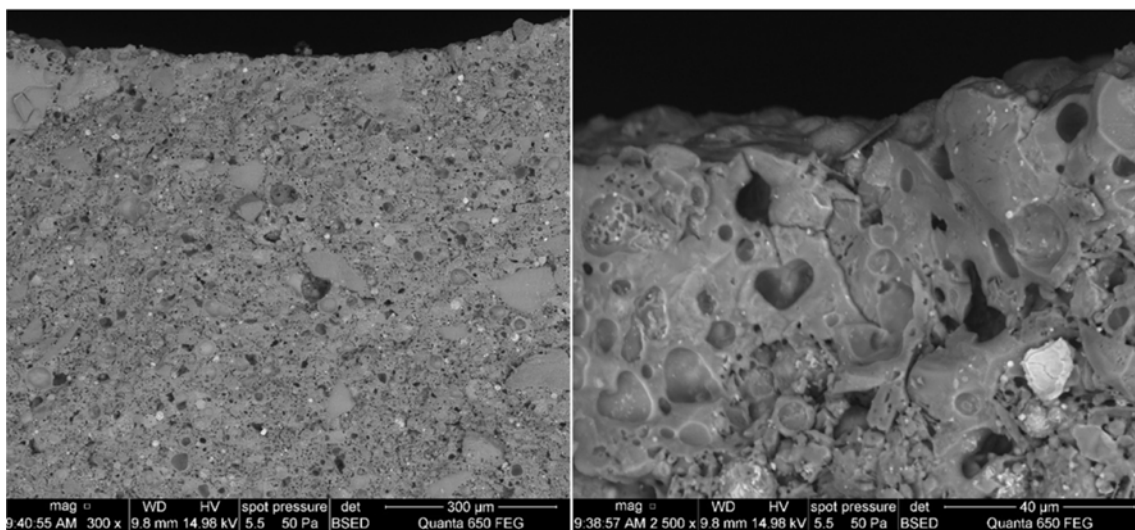


Fig. 3. Inner profile of the extruded tube after sintering.

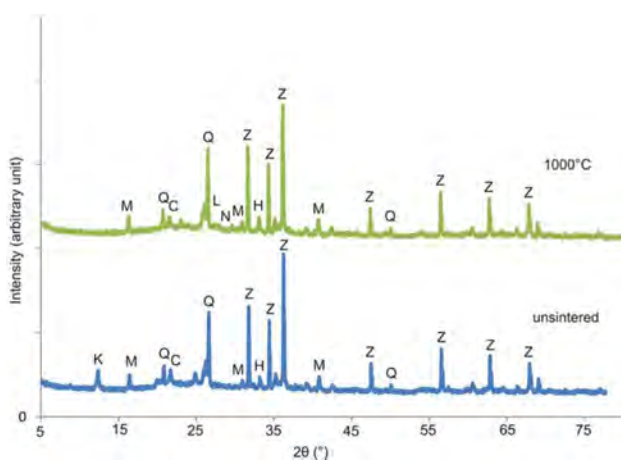


Fig. 4. XRD data for unsintered and sintered support. Quartz (Q), Zincite (Z), Mullite (M), Cristobalite (C), Hematite (H), Kaolinite (K), Nepheline (N).

technique for permeability study and therefore was used to describe the porosity and pore size distribution of the ceramic support. Fig. 5. shows the pore size distribution of the fly ash based support. The median pore diameter of the support was  $2.1 \mu\text{m}$  with an open porosity of 33%.

#### X-ray CT data processing

The default data for the 3D model of the microstructure is the series-sized 2D images of the studied ceramic support segment with the same size and the same starting point of the coordinate system. This data discretely describes the physical properties of the internal structure of the material of the scanned sample without distinction of individual objects. Imported digital monochrome 8-bit images are at resolution of  $1,096 \times 1,096$  pixels. The size of one pixel corresponds to a square of  $2.7 \mu\text{m}$  side length. Imported 2D images



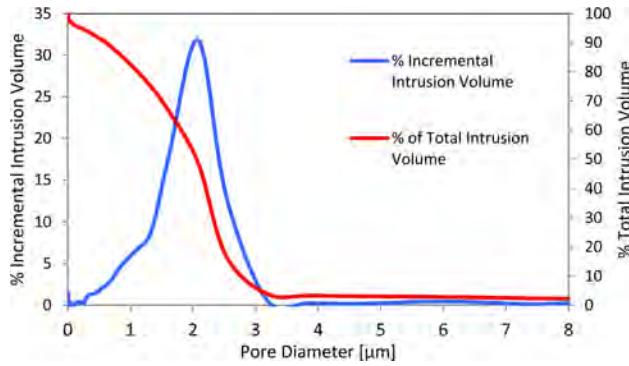


Fig. 5. Pore size distribution of the fly ash based support.

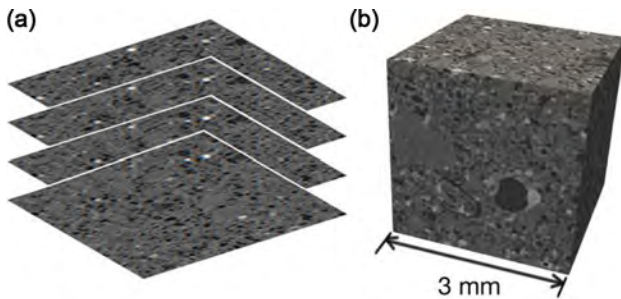


Fig. 6. (a) Example of the imported 2D images of the studied sample of the ceramic filter material and (b) the voxelized sample structure.

are placed vertically with a  $2.7 \mu\text{m}$  layer spacing and then converted to 3D so that each 2D pixel image is converted to a cubic voxel with a side length of  $2.7 \mu\text{m}$ . The total number of pictures taken is 1096. The part of the material segment used then corresponds to a  $27 \text{ mm}^3$  cube (Fig. 6).

#### Image histogram of processed 2D X-ray CT data

*Mathematical filter / Software: "Crop Geometry" / DREAM3D*

Imported X-ray CT images were subjected to mathematical analysis of the porous structure. The processing and analysis of digital images is done by mathematical operations common in the field of digital photography processing.

Firstly, it is necessary to perform so-called pre-processing consisting of sorting 2D CT images and cropping them on the area of interest. Cropping is necessary due to the microstructure spatial complexity and the large amount of input data. Images were cropped on a  $50 \times 50$  pixels ( $0.135 \times 0.135 \times 0.135 \text{ mm}$ ) cube in a randomly selected region of interest (ROI). See Fig. 7.

Sorted digital 2D images represent a three-dimensional matrix in which each point (pixel) with coordinates  $x, y$  is assigned the function value  $f$ . Functions  $f$ , resp. intensity of brightness corresponds to the gray scale information in the digital CT image. Depending on the color depth used, the function  $f$  values take the interval

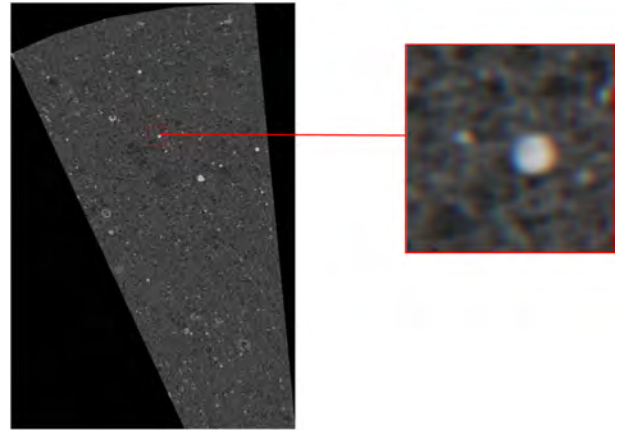


Fig. 7. Example of detail of the processed area, ROI  $50 \times 50$  pixels.

$f \in \langle 0, 1, \dots, n \rangle$ . When using an 8-bit resolution in a processed image, the luminance intensity functions are  $f \in \langle 0, 255 \rangle$  with 0 being black and 255 white.

The standard histogram, shown in Fig. 8, represents the layout of brightness level in a digital array matrix resulting from sorting and cropping a 2D CT image set. The histogram is a discrete function. The brightness intensities of each studied 2D image are in the interval  $\langle 0, L-1 \rangle$ , the  $L$  value being the highest grayscale value in a particular image. The discrete function then can be written as:

$$h(f_k) = n_k$$

where  $f_k$  are grayscale levels  $\langle 0, L-1 \rangle$ , and  $n_k$  is the pixel count with the brightness level of the  $f_k$  function.

The histogram, shown in Fig. 8, shows the frequency of the representation of the individual intensities in the three-dimensional sector processed. This histogram does not allow object and background distinction. This is due to the complex microstructure of the scanned sample from different pore depths, image artifacts and non-homogeneous composition of the material. The goal of the following math operations is to create a sharp interface between the objects and the background in the image.

#### Filtration of noise by linear averaging

*Mathematical filter / Software: "Mean (Kernel), Image Math" / DREAM3D*

Noise filtration is based on transforming an image by changing the brightness of the pixel of the input image to the brightness of the output image in order to highlight or suppress some of its properties. In the case of digital image processing of an irregular and complex material microstructure, this method is suitable for suppressing very small objects in the digital image, which have little effect on the resulting structural properties, and on the other hand highlighting large objects in the digital image.

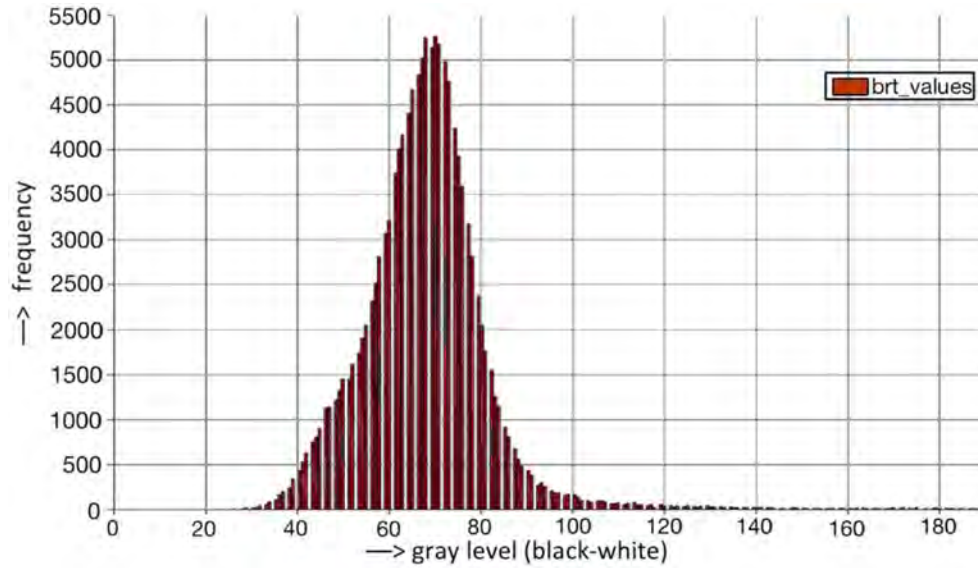


**Fig. 8.** Image histogram of the brightness intensity distribution in ROI  $50 \times 50$  pixels.

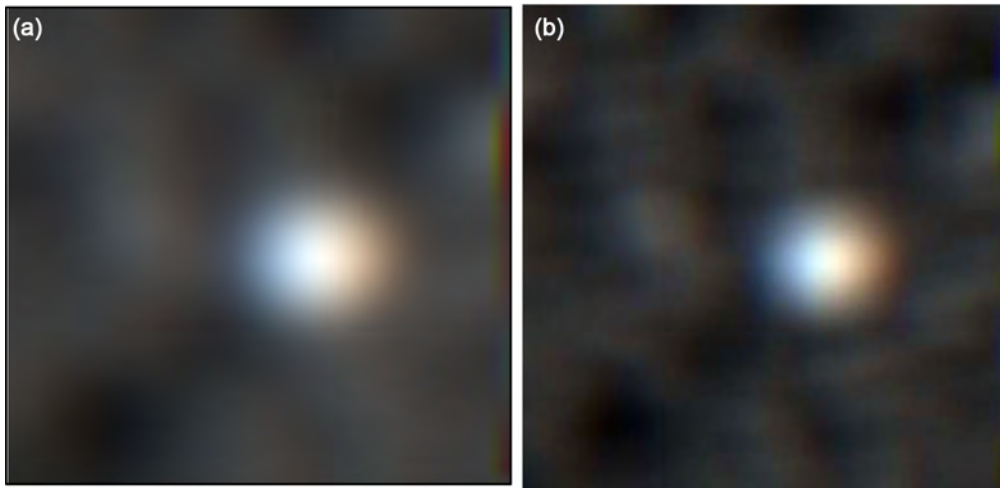


**Fig. 9.** Noise filtration by linear averaging - ROI  $50 \times 50$  pixels, (a) single, (b) triple.

The used image linear noise filtration gives satisfactory results when compared, for example, to a median or Gaussian filter. Using simple averaging filter involves assigning a new brightness value of function  $f$  at point  $x, y, z$  given by the arithmetic average of the brightness of the points in its vicinity. In the studied case, a ROI  $50 \times 50$  pixels was used. Linear filtering of noise suppresses image artifacts, but at the same time blurs the image, so the magnitude of the  $x, y, z$  diameter of the point should be less than the smallest detail studied in the scanned image. The new brightness function of each point in the three-dimensional image of the scanned sample can be written as:

$$f(x,y,z) = \frac{1}{m} * \sum_{k=1}^m g(x,y,z)$$

where  $m$  corresponds to the number of points in the

matrix, the function  $f$  the new value of the brightness of points in the matrix, and  $\Sigma$  functions  $g$  the sum of the brightness intensity values of the points in the original three-dimensional matrix. In this particular case, the noise removal using averaging filter needs to be done several times in succession, depending on the structure of the sample material being scanned (Fig. 9). For each processed segment of the scanned sample, it is necessary to approach each processing point individually depending on the local structure.

In Fig. 9(a) and (b) is shown a homogenization of the brightness intensity values in the image after noise filtration, making impossible to distinguish objects from the background in the histogram, or rather matter and pores in the material. It is therefore necessary to optimize the brightness intensity of the individual points by multiplying, see Fig. 10(a) and (b).

The essence of the algorithm is that each brightness

intensity point  $f$  is assigned a new value of the brightness intensity function  $h$ , given by the multiplicity of the original value of the function  $f$ :

$$h(x, y) = s * f(x, y)$$

The resulting image sharply distinguish the objects and the background, where the white areas represent the material of the sample being scanned, and the areas with different levels of gray represent the cavities in the structure.

Fig. 10(a) and (b) shows the studied section of the scanned image at various multiplication values of the function  $f$ . It is evident from the corresponding histogram (Fig. 8) that in this particular case, the most optimal combination of functions is triple linear averaging combined with five times the function  $f$  whose result is represented by Fig. 11(b).

**Image thresholding**

*Mathematical filter-Software: "Threshold Objects"/DREAM.3D*

The principle of thresholding is based on the assumption that the image has a different brightness value compared to its surroundings. The scanned black and white 2D CT image  $g(x, y)$  consists of a group of pixels, each pixel having an integer value of the brightness intensity function. Then the digital image can be written as  $m, n$  matrix:

$$A = \begin{bmatrix} a_{00} & \dots & a_{m0} \\ \vdots & \ddots & \vdots \\ a_{0n} & \dots & a_{mn} \end{bmatrix}$$

Then every point of this matrix can be written as a  $(m, n) = f(m, n)$ , where  $f$  is the function of the point (brightness, vector, etc.) and  $m, n$  are the coordinates of the point in the matrix. Mathematically, the image can

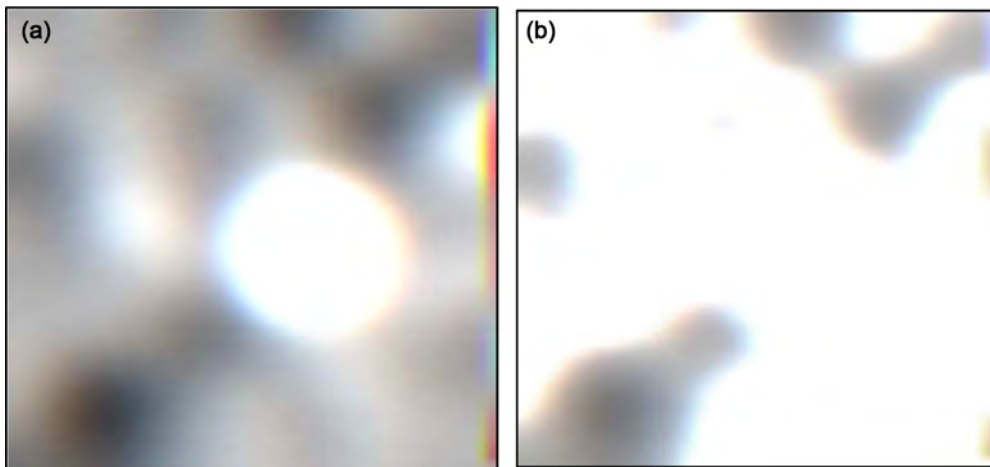


**Fig. 10.** Multiplication of the brightness after the three-fold linear averaging of the scanned image – ROI 50 × 50 pixels - (a) three times the intensity of the brightness, (b) five times the intensity of the brightness.

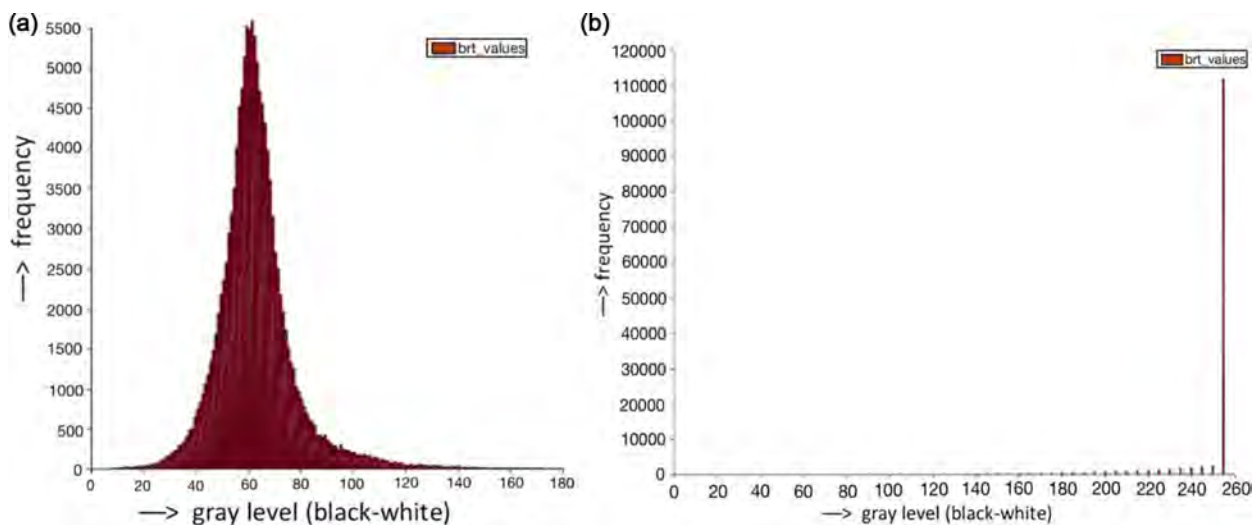


**Fig. 11.** Histogram of brightness intensity after noise filtration by triple linear averaging and multiplication of brightness intensity (a) three times the intensity of brightness, (b) five times the intensity of brightness.

be written as a matrix:

$$A = \begin{bmatrix} f_{00} & \dots & f_{m0} \\ \vdots & \ddots & \vdots \\ f_{0n} & \dots & f_{m2} \end{bmatrix}$$

In such a matrix, we select the thresholding function  $T$ . The function  $T$  is the so-called threshold corresponding to the pixels with the limit value of functions  $f$ , resp. intensity of brightness. Limit value of brightness defines whether it is a pixel object or background. In general, a threshold image can be defined as a:

$$g(x,y) = \begin{cases} 1 & f(m,n) > T \\ 0 & f(m,n) \leq T \end{cases}$$

The aforementioned function states that a pixel with a brightness intensity value greater than the threshold value  $T$  belongs to an object and a pixel with a brightness intensity value of less than or equal to the threshold value  $T$  belongs to the background. An algorithm based on this function scans every pixel and divides the pixels into two groups based on the thresholding function. The abovementioned approach is called simple thresholding and is applicable to scanned digital CT images consisting of one object and its background.

The thresholding function  $T$  according to Fig. 12(b) corresponds to a value of  $T < 254.5$ . Figures below depict the original X-ray-CT image of the studied ceramic material, the image after the filtering of the noise by linear filtration and the same image after thresholding

### Image segmentation

*Mathematical filter / Software "Segment Features (Scalar)"/DREAM.3D*

Image segmentation is the process of assigning a

label to every pixel in an image such that pixels with the same label share certain characteristics. Image segmentation algorithm so allows creating single objects that can be further extracted and processed.

The following description represents the schematic process of segmentation algorithm. In the matrix representing the digital CT image, the default pixels  $f(m, n)$  are randomly chosen in the region formed after the thresholding. The algorithm then searches for adjacent pixels, and based on the chosen absolute difference of brightness intensity function  $f$  of pixel  $m, n$  determines whether or not the pixel belongs to the selected region. The pixel belongs to the region if at least one pixel in its neighborhood acquires the absolute difference in brightness intensity at the selected interval.

When applied to a stack of images, the resulting contours after image segmentation can be used to create 3D reconstructions.

### Three-dimensional model processing

The principle of creating a three-dimensional model consists of converting a discrete description of the data obtained by mathematical analysis of 2D CT image data into vector descriptions. The vector description describes mathematically the outer structure of the surface of the studied object using the tetrahedral network. The modeling process consists of three steps, namely vectorization, smoothing and decimation of the surface.

#### Structural vectorization

*Mathematical filter / Software: "Quick Surface Mesh" / DREAM.3D*

Creating a surface mesh in DREAM.3D can currently be accomplished by using the Quick Surface Mesh Filter. The structural vectorization of surface created by the "marching cubes" method consists of creating a triangular network representing the surface of the studied object. This method is quick, because it simply

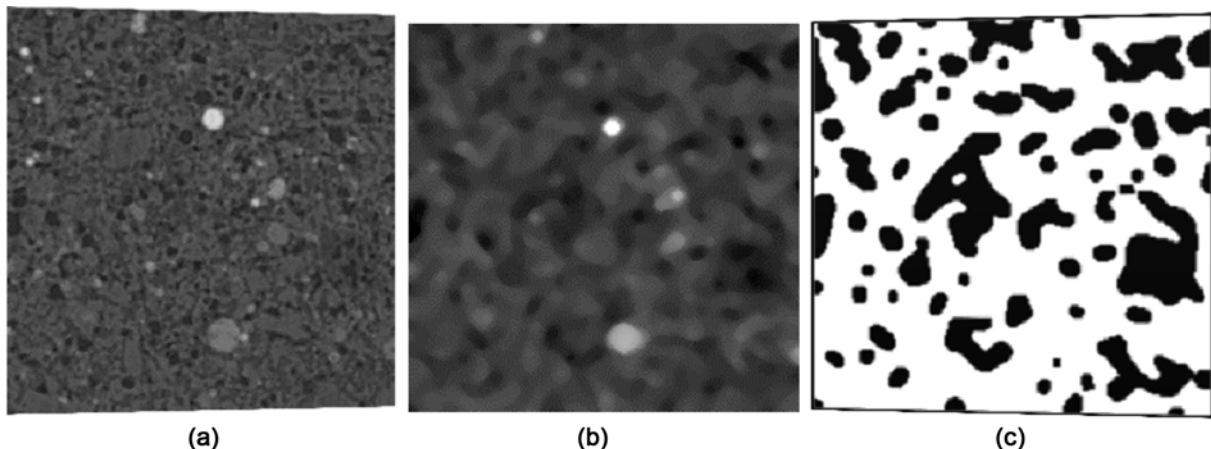


**Fig. 12.** (a) The original X-ray-CT image of the studied ceramic material, (b) the image after the filtering of the noise by linear filtration, (c) the same image after thresholding.



draws triangles across the voxel faces of an Image Geometry. The result is a Triangle Geometry, where the boundaries between Features are defined by connected triangles. This means that any given triangle is shared by two Features. The Triangle Geometry has a list of Sharp elements, where the elements are the primary unit element of the Geometry. For example, a Triangle Geometry has primary elements that are triangles with free vertices, so such a Geometry has a list of triangles that are defined by referencing the three vertex Ids of which they are composed [22]. The algorithm creates a pair of triangles on each cell side. The result is the tetrahedral cubic surface structure of the investigated material shown in Fig. 13.

The resulting surface mesh is usually not satisfactory, since it is remaining “blocky” from the original Image Geometry. Surface mesh smoothing using the Laplacian Smoothing Filter was used to solve this problem.

### Laplacian smoothing

*Mathematical filter / Software: “Laplacian Smoothing” / DREAM3D)*

Laplace's smoothing serves to smooth the cubic structure of the polygonal mesh. The algorithm's control parameter is the parameter  $\lambda$ , which defines the maximum allowed triangulation network node movement value. The factor  $\lambda$  is a small positive number. The Laplacian smoothing algorithm reduces the high frequency surface information and tends to flatten the surface. If  $\lambda$  is too small, one needs more iterations for smoothing and the smoothing process becomes time-consuming. If  $\lambda$  is not small enough, the smoothing process becomes unstable. In the Laplacian algorithm the  $\lambda$  term has a range of  $0 \leq \lambda \leq 1$  and defines a relative distance that a node can move relative to the positions of the node neighbours. A  $\lambda = 0$  value effectively stops these node types from any movement during the algorithm, so this allows this value to be set for specific types of nodes so that shrinkage of surface

mesh can be stopped during the smoothing process [22].

The shape and structure of the network after Laplace's smoothing is shown in Fig. 14.

### Surface decimation

*Mathematical filter / Software: “Decimate” / ParaView*

Smoothing the surface creates a network with a large number of triangles. This network is a very compute-intensive and so the decimating the surface takes place - while maintaining the shape and volume of the object as much as possible. The principle of surface decimation is to simplify the triangle mesh by reducing the number of triangles in such a way that overall origin shape of the mesh will be maintained intact. The control parameter is the percentage reduction in the number of triangles in the mesh (TargetReduction), resulting in a geometric error of the model, which is dependent on the mesh reduction ratio of the triangulation network. The decision parameter of the algorithm is the size of the minimum angle between the adjacent sides of the triangle (FeatureAngel). If this angle is equal to or less than the specified angle, its sides are considered to be an edge function and the network is divided here. The result of decimation of the triangulation network is shown in Fig. 15(a) and (b).

The obtained surface model was converted to a volume model using the Autodesk Inventor a 3D CAD construction software. Example of the resulting model suitable for analysis of material microstructure is shown in Fig. 16.

### Material structure information obtained from the created 3D model

In sections, 3 and 4 was described 3D reconstruction process from 2D image data from X-ray CT of the ceramic fragment. The overall reconstructed geometric model of the studied material space ( $3 \text{ mm}^3$ ) done by 3D CAD software by Autodesk is shown in Fig. 17.

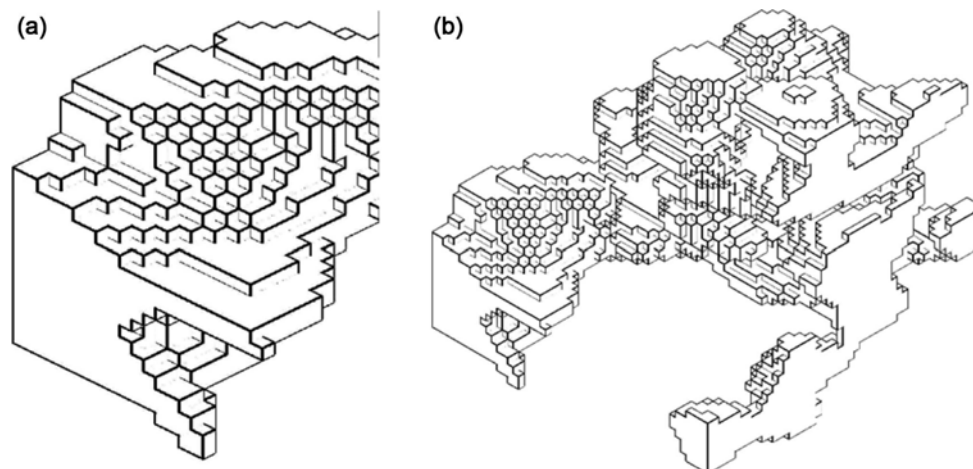


**Fig. 13.** Vectorization of the surface pore structures of material created by the “marching cubes algorithm” (a) detail, (b) matrix  $50 \times 50 \times 50$  voxels.

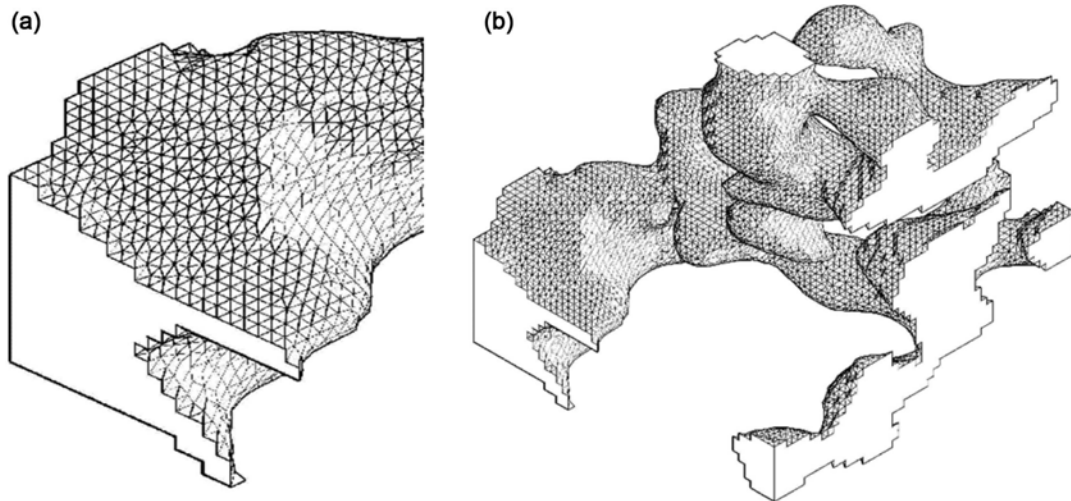


**Fig. 14.** Model of the pore surface structure after Laplace's smoothing (a) detail (b) matrix  $50 \times 50 \times 50$  voxels.

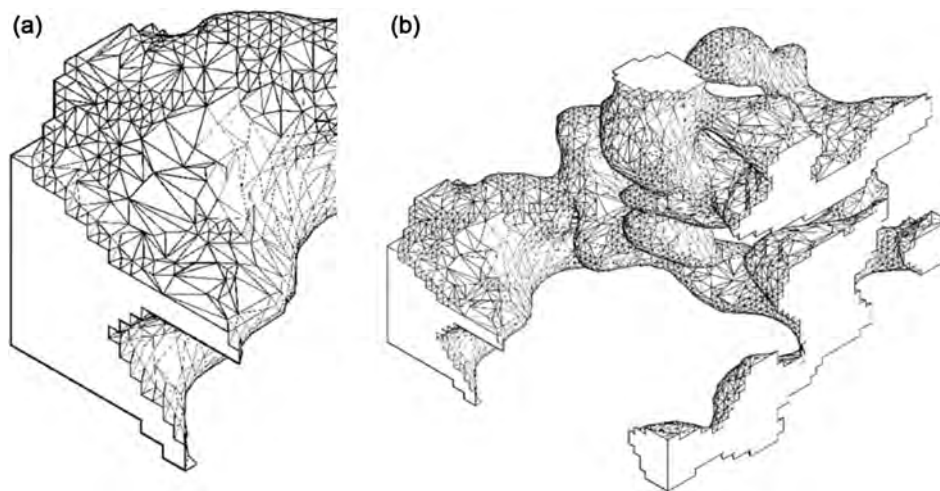


**Fig. 15.** Model of the pore surface structure after the Decimation algorithm (a) detail (b) matrix  $50 \times 50 \times 50$  voxels.

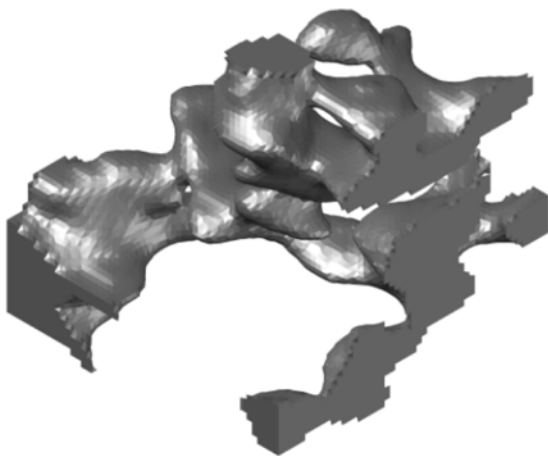


**Fig. 16.** The resulting model of pore structure created using the "mesh feature" algorithm in Autodesk Inventor.

Solid matrix of the material is depicted in red while the pores in grey.

Construction of 3D model is based on vector representation of fragmented data. Most common CAD softwares works with 3 types of model describes of single entities that forms future 3D structure. In such models could be included edge, surface or volume models. In this work has been used B-spline model with non-uniform rational B-spline surfaces that represent information about each surfaces forming network of the model. Each nod of the B-spline surface is defined by the defined weight value. Inner nodes are not defined, models work only with surface values.

The whole process is based on utilization on B-spline proces with focus on three specific steps. The first one is focused on vectorization and preparation of the vector network. By the approach of marching cubes is formed the coarse 3D surface. The used algoritmus gather raster voxel (eight of them) into the cube/prism. The second step is focused on spline procedure by which the algoritmus cutting the edges usually by the use of weight average of neighbor nodes. The last third

step provides reduction of polygonal surface structure and reduce number of nodes in term of production of the new surface with the same properties as the first coarse 3D surface between nodes. During the reduction process are set criteria that defends against significant changes in surface.

All that approaches has been videlly adopted in different CAD systems. Within this work has been used methods that maximally simplifies the whole process of 3D structure preparation.

Using the standard construction tools, it was possible to adjust the microstructure of material by extraction, rotation or separation of a specific object of interest. The mentioned operations were applied to the visual 3D model and allowed to evaluate the following properties of the ceramic support.

#### Porosity evaluation

Reconstructed model can be used for porosity evaluation. In created model, porosity results from comparison of solid matrix and inner porous space. Calculated ratio between the active porous area pores and the ceramic-forming material corresponded to porosity of 32%. Mercury porosimetry gives results of 33% (Section 2.1.6). If we take in account the uncertainties of both methods, values were in very

good agreement.

#### Evaluation of discontinuity

Industrial X-ray CT scanning usually serves for internal inspection of scanned material such as failure analysis and flaw detection. As for ceramic materials, typical flaws are represented by cracks. Defects in such materials are usually formed in large compact grains of the input material due to internal stresses during sintering and cooling process. Created model was visually inspected and areas of interest were separated from the object. On the Fig. 18. is depicted an example, where segment of interest (a) and its extracted part (b) represents cavity of dimension greater than  $10\ \mu\text{m}$ .

#### Homogeneity evaluation

Homogeneity is another parameter that can be studied visually by tracking a certain component with a specific characteristic. In our material, such components were cenospheres that form part of the power fly ash [24] used in prepared ceramic supports. The image (a) in Fig. 19. shows the 3D geometric model of silica-alumina microsphere with typical hollow, while image (b) shows the original 2D X-ray CT image. The 3D model (c) shows distribution of cenospheres in selected area to control the homogenization process of prepared

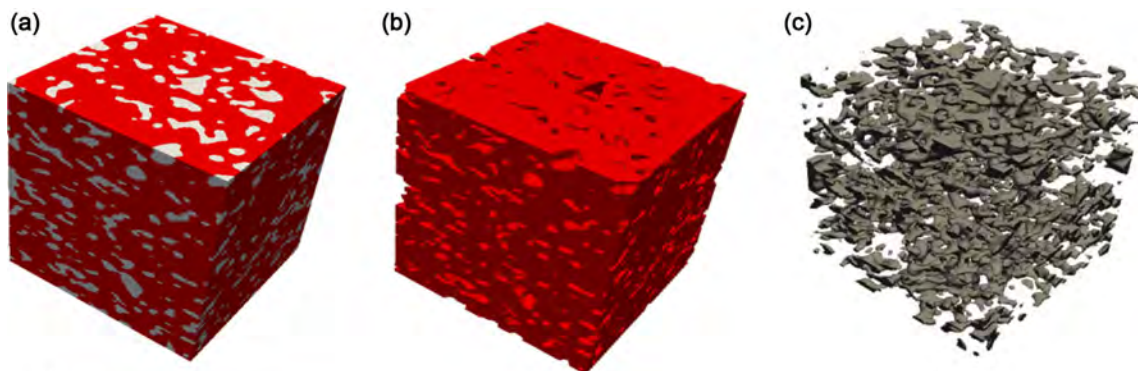


**Fig. 17.** (a) Images of the geometric model of the overall microstructure of the sample, (b) material structure, (c) pore structure. Cube edge length: 3 mm.

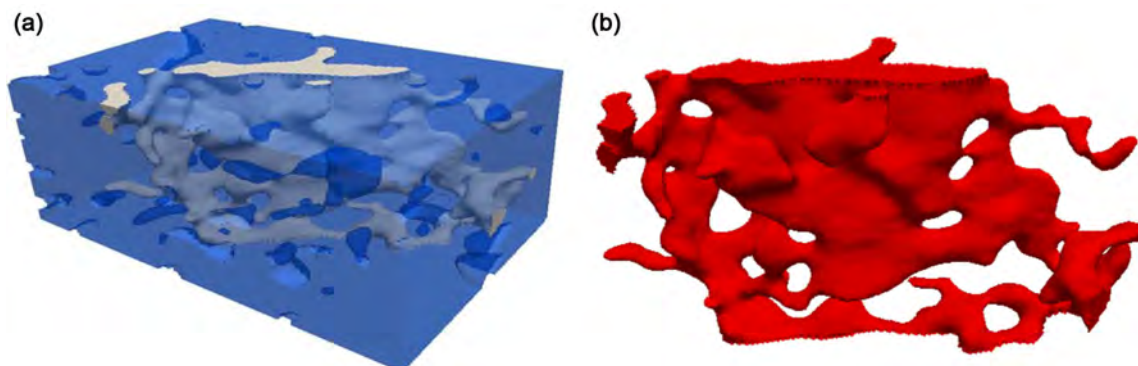


**Fig. 18.** (a) typical crack in the ceramic material, (b) isolated model of the cavity formed in the grain.

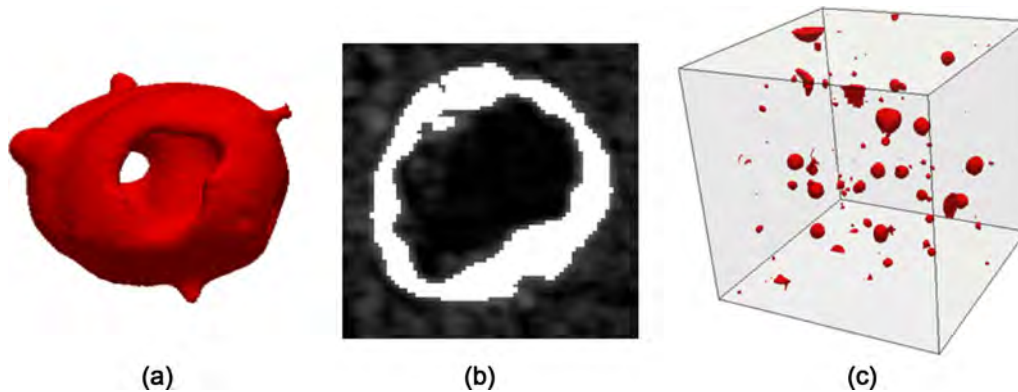


**Fig. 19.** (a) The 3D model of silica-alumina microspheres, (b) the original 2D X-ray-CT image, (c) distribution of cenospheres in selected area.

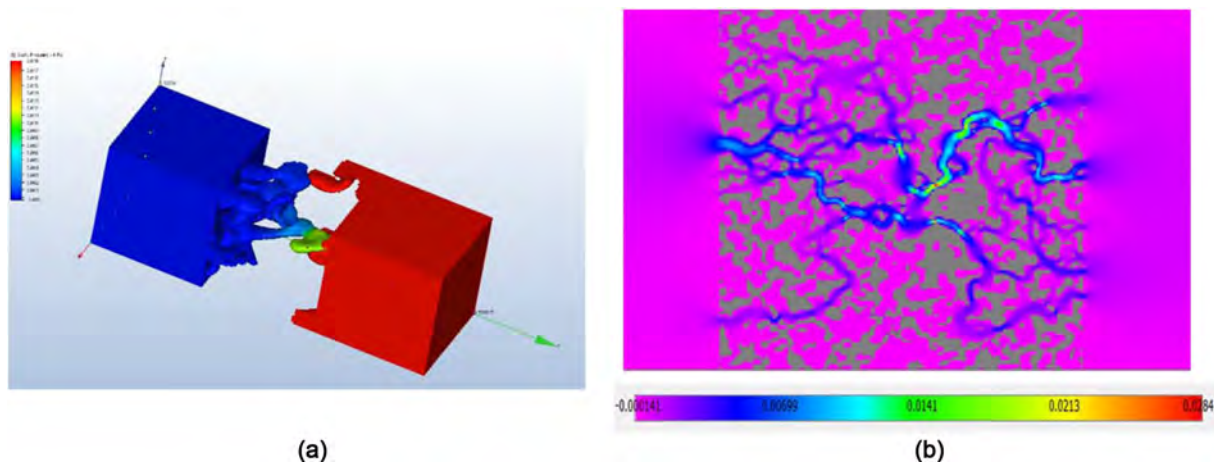


**Fig. 20.** Ceramic material model used for numerical simulation of flow (CFD) using the Navier Stokes equations (a) and lattice of the Boltzmann method (b)

ceramic support.

#### Geometric model for numerical simulation of flow

The output geometric 3D model can also be used for mathematical modelling of fluid transport through the structure of the material using the CFD (computational fluid dynamics) method. Numerical simulation is used as a tool for understanding the fluid flow mechanism and behaviour.

Fluid flow simulation through ceramic support micro-channels was performed using Autodesk CFD. The 3D model served for calculation as a medium in which liquid is introduced under specific conditions. The Fig. 20(a) shows the distribution of pressure conditions. From the initial state, the static pressure in and behind the channels increases due to the reduced flow environment. The Fig. 20(b) shows the flow velocity distribution. Due to the decreasing profile of the micro-channels, the gradient is increased in the constricted parts, which is released at the ends of the model. This also corresponds to the color scale.

#### Conclusion

The paper describes the process of creating a 3D model of the studied material from 2D X-ray CT image data. In this study, a sample of a newly prepared fly ash-based ceramic membrane support was examined to visualize its internal structure. The technique of spatial reconstruction of a three dimensional geometric model was made using the Paraview and DREAM.3D open source software. For image data reconstruction the image contrast adjusting algorithms, noise filtration by linear averaging, image thresholding and image segmentation algorithms have been used. The spatial reconstruction of the surface geometric model was performed using structural vectorization, Laplacian smoothing and surface decimation techniques. The surface model was then converted to a 3D model using the construction software Autodesk Inventor. The created virtual CAD model allows the isolation of individual objects with subsequent spatial analyses and so provides useful information about studied sample. The possibilities of using the 3D model for evaluation of total porosity, discontinuities, failures and defects, spatial



distribution of specific components in the material as well as for simulation of liquids flow were also outlined in the work.

In the summary, presented work provides operation instructions for data processing starting with CT scanning of examined porous ceramic material, through the mathematical analysis of 2D data and the creation of a 3D model to the examination of specific properties of the created object. The advantage is the visualization and spatial analysis of the internal structure of the newly created membrane support and related identification of weak spots and detection of various anomalies and thus enabling timely modification of production processes and/or input material. Using freely available software should contribute to expanding CT techniques among wider range of users.

### Acknowledgements

This work was done in connection with the Institute of Clean Technologies for Mining and Utilization of Raw Materials for Energy Use – sustainability programme. Identification code: LO1406. Project is supported by the National Programme for Sustainability I (2013-2020) financed by the state budget of the Czech Republic; the Project MPO Trio – FV20270 “Development of composite ceramic membranes based on recycled materials, including their application in the field of industrial wastewater cleaning and recycling” project funded by the state budget of the Czech Republic.

### References

1. M.C. Almandoz, C.L. Pagliero, and N.A. Ochoa, J. Marchese, *Ceram. Int.* 41 (2015) 5621-5633.
2. F. Bouzerara, A. Harabi, S. Achour, and A. Larbot, *J. Eur. Ceram. Soc.* 26 (2006) 1663-1671.
3. M.M. Bazin, N. Ahmad, and Y. Nakamura, *J. Asian. Ceram. Soc.* 7[4] (2019) 417-425.
4. P. Wu, Y. Xu, Z. Huang, and J. Zhang, *J. Ceram. Process. Res.* 16[1] (2015) 102-106.
5. M. Samaei, S. Gato-Trinidad, and A. Altaee, *Sep. Purif. Technol.* 200 (2018) 198-220.
6. V. Gitis and G. Rothenberg, in “Ceramic membranes: New Opportunities and Practical Applications” (John Wiley and Sons, 2016)
7. S.K. Hubadillah, M.H.D. Othman, T. Matsuura, A.F. Ismail, M.A. Rahman, Z. Harun, J. Jaafar, and M. Nomura, *Ceram. Int.* 44[5] (2018) 4538-4560.
8. S. Saja, A. Bouazizi, B. Achiou, M. Ouammou, A. Albizane, J. Bennazha, and S.A. Younssi, *J. Environ. Chem. Eng.* 6[1] (2018) 451-458.
9. J. Fang, G. Qin, W. Wei, and X. Zhao, *Sep. Purif. Technol.* 80 (2011) 585-591.
10. I. Jedidi, S. Saidi, S. Khemakhem, A. Larbot, N. Elloumi-Ammar, A. Fourati, A. Charfi, A.B. Salah, and R.B. Amar, *J. Hazard. Mater.* 172 (2009) 152-158.
11. Z. Harun, T.C. Ong, T. Matsuura, S.K. Hubadillah, M.H.D. Othman, and A. F. Ismail, *Chem. Eng. Res. Des.* 133 (2018) 111-125.
12. M. Arzani, H.R. Mahdavi, M. Sheikhi, T. Mohammadi, and O. Bakhtiari, *Appl. Clay Sci.* 161 (2018) 456-463.
13. B. Das, B. Chakrabarty, and P. Barkakati, *Ceram. Int.* 42[13] (2016) 14326-14333.
14. P. Iassonov, T. Gebrenegus, and M. Tuller, *Water Resour. Res.* 45 (2009) W09415.
15. H. Singh, and A.M. Gokhale, *Mater. Charact.* 54[1] (2005) 21-29.
16. D. Samak, A. Fisher, and D. Rittel, *CIRP ANN* 56[1] (2007) 149-152.
17. O. Wirjadi, in *Tech. Rep. Nr. 123, 2007*, edited in Fraunhofer ITWM, Kaiserslautern, Germany.
18. T. Li, X. Lu, B. Wang, Z. Wu, K. Li, D.J.L. Brett, and P.R. Shearing, *J. Membr. Sci.* 528 (2017) 24-33.
19. E. Gregorová, T. Uhlířová, W. Pabst, P. Diblíková, and I. Sedlářová, *Ceram. Int.* 44[11] (2018) 12315-12328.
20. H. Taud, R. Martinez-Angeles, J. F. Parrot, and L. Hernandez-Escobedo, *J Petrol Sci Eng.* 47[3-4] (2005) 209-217.
21. [www.paraview.org](http://www.paraview.org)
22. <http://dream3d.bluequartz.net/>
23. J. Davidovits, in 4<sup>th</sup> edition *Geopolymer Chemistry and Application*, November 2015, published by Institut Geopolymere, France.
24. M. Zyrkowski, R.C. Neto, L.F. Santos, and K. Witkowski, *Fuel* 174 (2016) 49-53.